Experimental Evidence for the Intimate Interaction among Sheared Flows, Eddy Structures, Reynolds Stress, and Zonal Flows across a Transition to Improved Confinement

I. Shesterikov,[1,†] Y. Xu,[1,*] G. R. Tynan,[2] P. H. Diamond,[2] S. Jachmich,[1] P. Dumortier,[1] M. Vergote,[1] M. Van Schoor,[1] G. Van Oost,[3] and TEXTOR Team

[1]*Laboratoire de Physique des Plasmas-Laboratorium voor Plasmafysica, Association Euratom-Belgian state, Ecole Royale Militaire-Koninklijke Militaire School, B-1000 Brussels, Belgium*

[2]*University of California, San Diego, 9500 Gilman Drive, La Jolla, California 92093, USA*

[3]*Department of Applied Physics, Ghent University, B-9000 Ghent, Belgium*

(Received 28 March 2013; published 1 August 2013)

Dedicated experiments have been carried out at the TEXTOR tokamak in biasing-induced improved confinement regimes using Langmuir probe and GPI measurements. The results show the first evidence for the intimate interaction among sheared flows, eddy structures, Reynolds stress, zonal flows, and ambient fluctuations during a transition to an improved confinement. The sheared flows impose dynamic effects on turbulence structures, resulting in generation of Reynolds stress and zonal flows and eventually the suppression of background fluctuation levels via nonlinear energy transfer processes. The latter may therefore trigger a transition to the H mode.

DOI: 10.1103/PhysRevLett.111.055006 PACS numbers: 52.70.Kz, 52.25.Xz, 52.35.Ra, 52.55.Fa

It is generally believed that the high energy confinement (H mode) is attributed to radially sheared $E_r \times B$ flows in decorrelating turbulence eddies [1,2]. The relation between the $E_r \times B$ flow shear and the H mode has been affirmed in continuous current tokamak and TEXTOR tokamaks [3,4], where edge flows were generated using biasing electrodes. Recently, several experiments indicated that the zonal flows play a crucial role in triggering the transition to H mode [5–7]. According to theories, the zonal (mean) flows can be generated by Reynolds stress via symmetry breaking of eddies [8,9]. However, hitherto a complete picture of the dynamic interaction among mean (zonal) flows, eddy structures, and Reynolds stress across the transition has not yet been achieved. In this work, we have performed dedicated experiments at TEXTOR by actively controlling the $E_r \times B$ shear rate in biasing experiments, in which we first reached H mode at a certain biasing voltage (V_{bias}) and then tuned V_{bias} at different levels to explore the underlying physical processes. Meanwhile, we utilized two sets of high spatiotemporally resolved diagnostics [Langmuir probes and gas-puff imaging (GPI)], especially the GPI to directly observe the 2D structure of turbulence eddies [10]. In this Letter, we present the first experimental observation for the intimate interplay between flow shears and eddy structures during the transition to an improved confinement.

The experiments were executed in Ohmic deuterium discharges at TEXTOR ($R = 175$ cm, $a \approx 47.5$ cm). Plasma current $I_p = 250$ kA, toroidal magnetic field $B_T = 1.6$ T and 2.25 T and the line-averaged density $\bar{n}_e = (1.5\text{–}2.3) \times 10^{19}$ m^{-3}. To generate an edge radial electric field E_r and an $E_r \times B$ flow shear layer, a positive V_{bias} (0–250 V) has been imposed between an electrode (inserted at $r \approx 43$ cm) and the toroidal limiter. Although locally biased, the electrode generates an equal electric potential at that radius across the whole magnetic flux surface, and hence, affects the E_r globally. The edge equilibrium and fluctuating quantities were measured by fast reciprocating probes mounted at the outer midplane [11]. The sampling frequency is 500 kHz. For visualizing the 2D (radial vs poloidal) turbulence structures, a GPI diagnostic is also installed at the outer midplane and toroidally 40° away from the probes [10,12]. The view field of the GPI [covering both the plasma edge and the scrape-off layer] is $\sim 12 \times 12$ cm^2 with a frame rate of 2 μs.

Typical discharge waveforms of a biasing-triggered H mode are plotted in Fig. 1. In Fig. 1(a) the solid curve shows the time evolution of the biasing voltage with a maximal value ($V_{\mathrm{bM}} = 250$ V). The V_{bias}, ramping almost linearly from 0 to 250 V and then holding constant for ~ 0.6 s, was applied in the stationary discharge stage. During the ramping phase, a transition of plasma confinement to H mode occurs at $V_{\mathrm{bias}} \cong 130$ V (see the vertical dashed line), along with an increase in $\bar{n}_e$ and a reduction in the D_α signal [see Fig. 1(b)]. The transition threshold of V_{bias} has been confirmed in other biasing discharges, e.g., for $V_{\mathrm{bM}} = 150$ V, Figs. 1(a) and 1(b) show similar transition to H mode at $t = 2.38$ s, when $V_{\mathrm{bias}} \approx 130$ V. Obviously, to unravel the L-H transition mechanisms and interaction between flows and turbulence, the ramping phase in V_{bias} should be the focus of our studies, i.e., trace the changing of related quantities at the time of A, B, C, D, E during the rising period of V_{bias}. Whereas the probe measurements can cover the entire rising period of V_{bias}, the GPI can only expose about 0.6 ms in one discharge because of a limited number of the camera frames [10]. Thus, the GPI cannot detect continuously the changing of turbulence from A to E in one shot. Alternatively, we made

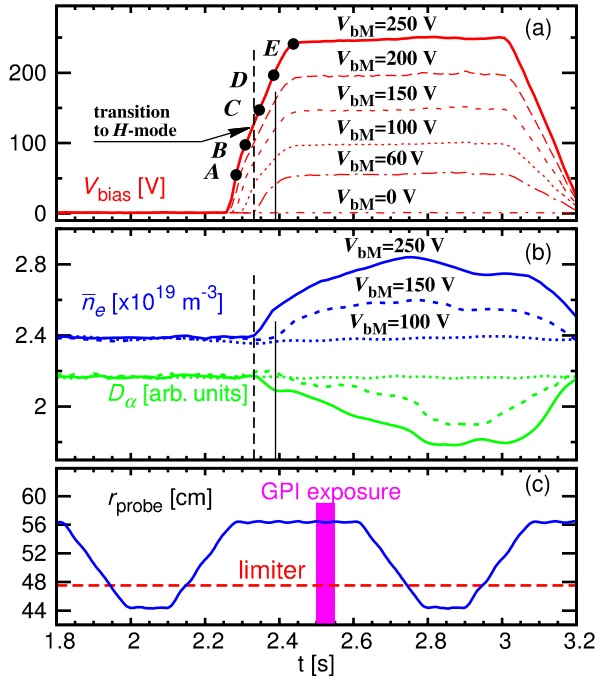

FIG. 1 (color online). Typical waveforms of biasing H-mode discharges at TEXTOR. Time traces of (a) biasing voltages V_{bias} in different V_{bM} discharges; (b) $\bar{n}_e$ and D_α emission on the limiter in three V_{bM} shots; (c) radial position of reciprocating probes and the GPI exposure time window.

a stepwise increase of the maximal V_{bM} shot by shot (under the same discharge condition) from 0 to 60, 100, 150, 200, 250 V. These V_{bM} are equal to the V_{bias} values at the time of A, B, C, D, E. Figure 1(c) shows the time trace of the fast probe, moving from the scrape-off layer into the plasma inside the last closed flux surface. For a comparison before and during the biasing, the fast probe plunges twice in one discharge. The vertical pink color bar marks the GPI exposure time in the H-mode phase.

The radial profiles of E_r have been measured by probes from the plasma potential $V_p = V_f + 2.8T_e$, where V_f (floating potential) and T_e (electron temperature) are measured by a triple probe [13]. The results are plotted in Fig. 2(a) for various V_{bM} shots. Figure 2(b) depicts the corresponding radial profiles of the $E_r \times B$ flow shear rate, $\omega_s = (\partial E_r/B\partial r)$. As the V_{bM} increases from 0 to 250 V,

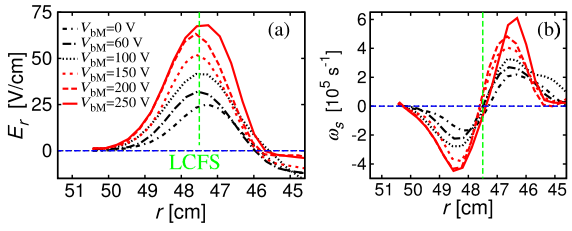

FIG. 2 (color online). Radial dependence of (a) E_r and (b) $E_r \times B$ flow shear (ω_s) in different V_{bM} shots.

both E_r and ω_s gradually increase nearby the last closed flux surface.

Figures 3(a) and 3(b) show typical GPI images in two biasing discharges. Here we subtracted the time-averaged intensity for each image to get turbulent quantities. In Fig. 3(a) when $V_{bM} = 0$ the eddy shape is close to circular, while in Fig. 3(b) the eddies are stretched with a tilted angle ϕ as the V_{bM} increases to 60 V. To further characterize the eddy shapes, a two-dimensional space fast Fourier transform has been used. Figures 3(c) and 3(d) plot 2D wave number spectra (k_r vs k_θ) for the GPI images in Figs. 3(a) and 3(b). Similar to the images, the wave number spectra are quasisymmetric and asymmetric in Figs. 3(c) and 3(d), respectively.

To detect the dynamical evolution of eddy structures at different flow shear rates, we have analyzed the variation of eddy shapes in a series of discharges (with different V_{bM}) across the transition, as illustrated in Fig. 1. For each V_{bM}, the ratio of ω_s to the natural scattering rate of turbulence, ω_D (inferred from the autocorrelation of potential fluctuations where the $E_r \times B$ flow ≈ 0), has been estimated and shown on the top of Fig. 4 for various V_{bM} shots. Figures 4(a)–4(f) show the contour plots of 2D wave number spectra. Each spectrum is averaged over 300 images in every shot. When $V_{bM} = 0$, the ratio $\omega_s/\omega_D \approx 1.2$ and the $k_r - k_\theta$ spectrum is roughly symmetric. When ω_s/ω_D is enhanced up to 1.5 and 1.8 ($V_{bM} = 60$ V, 100 V), the spectrum becomes elliptic due to continuous tilting effects on initially circular eddy structures. Similar phenomena have been observed in TJ-II, NSTX, and LAPD devices [14,15]. As the V_{bM} exceeds the transition threshold ($V_{bias} \geq 130$ V) and further increases from 150 V to 250 V, the spectrum becomes wider and less stretched. The widening of the spectrum implies the breakup of eddies when $\omega_s/\omega_D \geq 2.0$, as we observed

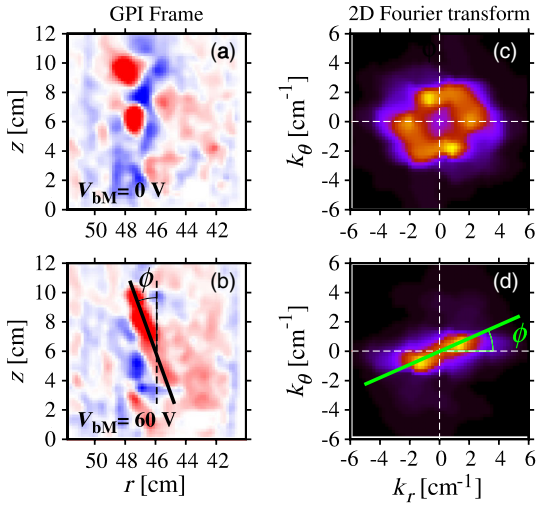

FIG. 3 (color online). (a)–(b) GPI frames and (c)–(d) their 2D wave number spectra measured in two V_{bM} discharges. (a), (c) $V_{bM} = 0$ V and (b), (d) $V_{bM} = 60$ V.

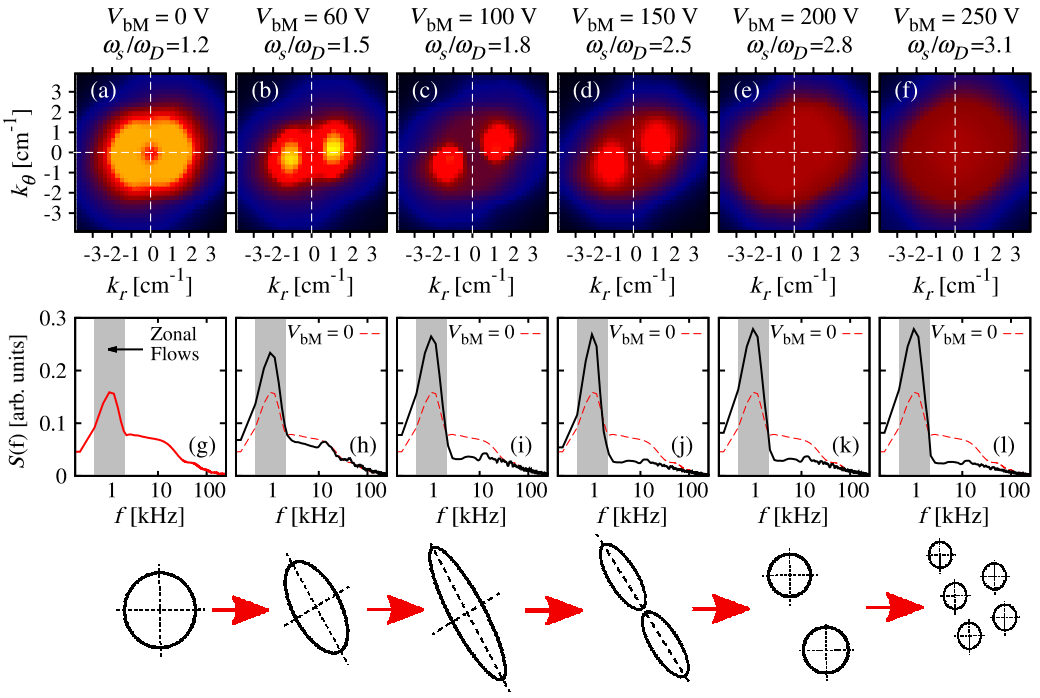

FIG. 4 (color online). (a)–(f) Contour plots of 2D wave number spectra in different V_{bM} shots. (g)–(l) Frequency spectra of potential fluctuations. The red dashed curve is the spectrum for $V_{bM} = 0$. Bottom row: A schematic view of the eddy shape under different V_{bM}.

earlier [10]. Apparently, the stretching of eddies is less effective once the large structure is broken into small pieces. A schematic view of the eddy shape with increasing V_{bM} and ω_s is depicted at the bottom of Fig. 4.

The second row in Fig. 4 plots the change in the fluctuation level with increasing ω_s in various V_{bM} discharges. Shown in Figs. 4(g)–4(l) are the frequency spectra [$S(f)$] of potential fluctuations measured by probes at $r \approx 47$ cm in the shear layer. When $V_{bM} = 0$ V, the $S(f)$ displays small coherent modes ~1.3 kHz, associated with low frequency zonal flow (LFZF) [16]. As the ω_s increases with enhanced V_{bM}, the fluctuation power at high frequencies is reduced in comparison with the initial one, as marked by the red dashed curve. These results are in agreement with the shear decorrelation on small-scale turbulence. However, for the LFZF, their fluctuation power is strongly amplified with the increase of V_{bM} from 0 to 100 V and then saturated at higher V_{bM} after transition to H mode.

Given the fact that the zonal flows are induced by Reynolds stress (RS) due to the breaking of the symmetrical spectrum of turbulent eddies [8,9], it is interesting to investigate the change in RS across the transition. To this end, an optical flow approach [17] has been applied to the GPI data to reconstruct the 2D fluctuating velocity vector fields, $\tilde{v}_r$ and $\tilde{v}_\theta$, by which we can compute the RS by $\langle \tilde{v}_r \tilde{v}_\theta \rangle$. Figure 5(a) shows radial profiles of the RS derived in different V_{bM} shots from 0 to 200 V. For $V_{bM} = 250$ V, the reconstruction of velocity fields is unreliable because of poor continuity in the GPI frame data [17]. It can be seen that (i) at zero V_{bM}, the RS and its radial gradient are both small, (ii) when V_{bM} is increased to 60 V and 100 V, the RS and its gradient become much larger, in accordance with the stretched shape of eddies, and (iii) with further increasing of V_{bM} from 150 to 200 V, the RS gradually diminishes due to recovery of the symmetry of eddy structures after splitting. The buildup of the RS for $V_{bM} = 0$–100 V could be relevant as a driving mechanism for the LFZF, as predicted in [18].

For a deep understanding of the H-mode transition physics, the nonlinear energy transfer between the ambient turbulence (AT) and the amplified LFZF prior to the transition should be further inspected. For this purpose, a simple model of the power balance between small-scale AT and large-scale zonal flows [19] has been applied:

$$\frac{\partial \tilde{v}_{\text{turb}}^2}{\partial t} = \gamma_{\text{eff}} \tilde{v}_{\text{turb}}^2 - \gamma_{\text{decor}} \tilde{v}_{\text{turb}}^2 + \frac{\partial \langle \tilde{v}_r \tilde{v}_\theta \rangle}{\partial r} V_{\text{ZF}}, \quad (1)$$

$$\frac{\partial V_{\text{ZF}}^2}{\partial t} = -\frac{\partial \langle \tilde{v}_r \tilde{v}_\theta \rangle}{\partial r} V_{\text{ZF}} - \mu_{\text{ZF}} V_{\text{ZF}}^2 \quad (2)$$

where $\tilde{v}_{\text{turb}}^2$ and V_{ZF}^2 represent, respectively, the turbulent and zonal flow energies, γ_{eff} and γ_{decor} are the turbulence energy input rate (driven by $\nabla n, \nabla T, \ldots$) and decorrelation rate towards AT, respectively, and μ_{ZF} the damping rate of zonal flows. This model essentially reveals a predator-prey process for the energy transfer between the AT and the LFZF. Figure 5(b) plots time traces of the poloidal $E_r \times B$ velocity ($V_{E\times B}$) and the AT energy ($\tilde{v}_{\text{turb}}^2$ in a frequency range 20–200 kHz), both measured by probes at $r =$ 46.5 cm with $V_{bM} = 150$ V. The oscillation in $V_{E\times B}$

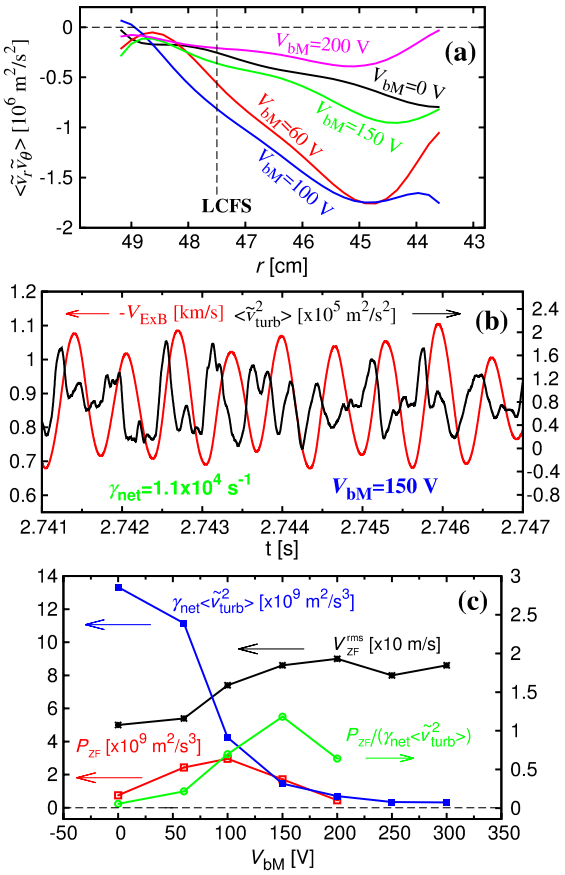

FIG. 5 (color online). (a) Radial profiles of Reynolds stress measured by GPI at different V_{bM} discharges. (b) Time traces of the turbulence energy and the $V_{E\times B}$ velocity at $V_{bM} = 150$ V. (c) The energy transfer parameters in the power balance model as a function of V_{bM}.

reflects the zonal flow (V_{ZF}) oscillation at $f \cong 1.3$ kHz. The $\tilde{v}^2_{turb}$ is also varying at the same frequency and correlated well with the V_{ZF} variations. The small phase delay ($\approx \pi/2$) in between corresponds to a limit cycle oscillation in the predator-prey regime [6,7]. Equation (1) indicates that the growth or drop of the AT energy depends on the competition between net effective power input $\gamma_{net} \cdot \tilde{v}^2_{turb}$ ($\gamma_{net} = \gamma_{eff} - \gamma_{decor}$) and nonlinear power transfer $P_{ZF} = \partial\langle\tilde{v}_r\tilde{v}_\theta\rangle/\partial r \cdot V_{ZF}$, namely, the effective power transfer rate, $P_{ZF}/(\gamma_{net}\langle\tilde{v}^2_{turb}\rangle)$. According to Eq. (1), the net effective power input can be deduced from the time derivative of the AT energy ($\partial\tilde{v}^2_{turb}/\partial t$), when $V_{ZF} = 0$. Assuming that this net power input changes little with or without V_{ZF} [19], we estimated from Fig. 5(b) an averaged value of $\gamma_{net} \cdot \tilde{v}^2_{turb} \approx 1.45 \times 10^9$ m^2/s^3 and $\gamma_{net} = 1.1 \times 10^4$ s^{-1} from the raising phases of the $\tilde{v}^2_{turb}$ signal at the time of minimal $V_{E\times B}(V_{ZF} \cong 0)$. Meanwhile we calculated $P_{ZF} = 1.72 \times 10^9$ m^2/s^3 from the RS gradient at $r \approx 46.5$ cm and the rms level of the V_{ZF} signal (V^{rms}_{ZF}). Hence, we obtained the effective power transfer rate, $P_{ZF}/(\gamma_{net} \cdot \langle\tilde{v}^2_{turb}\rangle) \approx 1.18$ in case of $V_{bM} = 150$ V. Using a similar way, we computed these relevant quantities in different biasing scenarios. The results are depicted in Fig. 5(c), where the V^{rms}_{ZF}, P_{ZF}, $\gamma_{net} \cdot \tilde{v}^2_{turb}$ and $P_{ZF}/(\gamma_{net} \cdot \langle\tilde{v}^2_{turb}\rangle)$ are plotted as a function of V_{bM}. With increasing V_{bM}, $\gamma_{net} \cdot \tilde{v}^2_{turb}$ decreases rapidly while V^{rms}_{ZF} gradually increases and saturates after $V_{bM} = 150$ V. Interestingly, because of maximal eddy tilting and the resultant RS gradient, the P_{ZF} shows a local maximum at $V_{bM} = 100$ V and the effective power transfer rate reaches to unity at $V_{bM} = 150$ V. Note that the transition to H mode takes place at $V_{bias} = 130$ V. These results clearly demonstrate the key role that energy transfer plays in triggering a transition to improved confinement. At higher biasing voltage ($V_{bM} \geq 150$ V), the P_{ZF} decreases with reduction of the RS gradient. However, the V_{ZF} itself persists due to the reduced parallel viscosity for zonal flow damping in toroidal plasmas [20,21].

Now we get the entire physical picture as follows: at the initial stage, with increasing flow shear the eddies are stretched and the RS increases due to the symmetry breaking mechanism. Concurrently, the zonal flows are excited by enhanced RS and extract energy from AT via nonlinear energy transfer. As the power transfer rate approaches unity, the plasma confinement is improved and transits into the H mode. When the ω_s further increases in the H mode, the eddies split into small pieces that are symmetric in shape and the RS diminishes. However, the zonal flows remain robust while background fluctuations are suppressed.

In conclusion, dedicated experiments have been conducted at TEXTOR in biasing H-mode experiments. In this Letter, we present the first evidence of the eddy stretching and splitting process in a confinement device and the intimate interaction between sheared flows and eddy structures. The results may have significant implication for the understanding of L-H transition physics.

We acknowledge valuable comments from T. Carter, E. Gusakov, G. Morales, M. Ramisch, and the technical support from K. Klören, B. Schweer, D. Nicolai and the whole TEXTOR team. I. Shesterikov thanks A. Tabula for continuous encouragement.

*Corresponding author.
y.xu@fz-juelich.de
†Corresponding author.
i.shesterikov@fz-juelich.de

[1] H. Biglari, P. H. Diamond, and P. W. Terry, Phys. Fluids B **2**, 1 (1990).
[2] K. H. Burell, Phys. Plasmas **4**, 1499 (1997).
[3] R. J. Taylor, M. Brown, B. Fried, H. Grote, J. Liberati, G. Morales, P. Pribyl, D. Darrow, and M. Ono, Phys. Rev. Lett. **63**, 2365 (1989).
[4] R. Weynants *et al.*, Nucl. Fusion **32**, 837 (1992).
[5] G. Conway C. Angioni, F. Ryter, P. Sauter, and J. Vicente, Phys. Rev. Lett. **106**, 065001 (2011).

[6] T. Estrada, C. Hidalgo, T. Happel, and P. H. Diamond, Phys. Rev. Lett. **107**, 245004 (2011).
[7] L. Schmitz, L. Zeng, T. L. Rhodes, J. C. Hillesheim, E. J. Doyle, R. J. Groebner, W. A. Peebles, K. H. Burrell, and G. Wang, Phys. Rev. Lett. **108**, 155002 (2012).
[8] E.-J. Kim and P. Diamond, Phys. Plasmas **10**, 1698 (2003).
[9] O. D. Gürcan, P. H. Diamond, T. S. Hahm, and R. Singh, Phys. Plasmas **14**, 042306 (2007).
[10] I. Shesterikov, Y. Xu, C. Hidalgo, M. Berte, P. Dumortier, M. Van Schoor, M. Vergote, and G. Van Oost, Nucl. Fusion **52**, 042004 (2012).
[11] Y. Xu *et al.*, Nucl. Fusion **47**, 1696 (2007).
[12] I. Shesterikov *et al.*, in *39th EPS Conference on Plasma Physics and 16th ICPP, Stockholm, Sweden, 2012* (European Physical Society, Mulhouse, 2012), p. P5.064.
[13] S. Chen, and T. Sekiguchi, J. Appl. Phys. **36**, 2363 (1965).
[14] J. A. Alonso *et al.*, Plasma Phys. Controlled Fusion **48**, B465 (2006).
[15] T. Carter, and J. E. Maggs, Phys. Plasmas **16**, 012304 (2009).
[16] Y. Xu, S. Jachmich, R. R. Weynants, M. Van Schoor, M. Vergote, A. Kramer-Flecken, O. Schmitz, B. Unterberg, C. Hidalgo, and TEXTOR Team, Phys. Plasmas **16**, 110704 (2009).
[17] T. Munsat, and S. J. Zweben, Rev. Sci. Instrum. **77**, 103501 (2006).
[18] P. H. Diamond, Y.-M. Liang, B. Carreras, and P. Terry, Phys. Rev. Lett. **72**, 2565 (1994).
[19] G. Tynan *et al.*, in *24th IAEA Fusion Energy Conference, San Diego, USA, 2012* (IAEA, Vienna, 2013), pp. EX/10–3.
[20] S. V. Novakovski, C. S. Liu, R. Z. Sagdeev, and M. N. Rosenbluth, Phys. Plasmas **4**, 4272 (1997).
[21] A. Fujisawa, Nucl. Fusion **49**, 013001 (2009).